RESEARCH ARTICLE

Benchmarking the proteomic profile of animal models of mesial temporal epilepsy

Amanda M. Canto[1,2] (iD), Alexandre B. Godoi[1,2] (iD), Alexandre H. B. Matos[1,2], Jaqueline C. Geraldis[1,2], Fabio Rogerio[2,3], Marina K. M. Alvim[2,4], Clarissa L. Yasuda[2,4], Enrico Ghizoni[2,4], Helder Tedeschi[2,4], Diogo F. T. Veiga[1,2], Barbara Henning[1,2], Welliton Souza[1,2], Cristiane S. Rocha[1,2], André S. Vieira[2,5], Elayne V. Dias[2,5], Benilton S. Carvalho[2,6], Rovilson Gilioli[7], Albert B. Arul[8], Renã A. S. Robinson[8], Fernando Cendes[2,4] & Iscia Lopes-Cendes[1,2] (iD)

[1]Department of Translational Medicine, School of Medical Sciences, University of Campinas (UNICAMP), Campinas, SP, Brazil
[2]Brazilian Institute of Neuroscience and Neurotechnology (BRAINN), Campinas, SP, Brazil
[3]Department of Pathology, School of Medical Sciences, University of Campinas (UNICAMP), Campinas, SP, Brazil
[4]Department of Neurology, School of Medical Sciences, University of Campinas (UNICAMP), Campinas, SP, Brazil
[5]Department of Structural and Functional Biology, Institute of Biology, University of Campinas (UNICAMP), Campinas, SP, Brazil
[6]Department of Statistics, Institute of Mathematics, Statistics and Scientific Computing, University of Campinas (UNICAMP), Campinas, SP, Brazil
[7]Laboratory of Animal Quality Control, University of Campinas (UNICAMP), Campinas, SP, Brazil
[8]Department of Chemistry, Vanderbilt University, Nashville, Tennessee, 37235, USA

Correspondence
Iscia Lopes-Cendes, Department of Translational Medicine, School of Medical Sciences, University of Campinas (UNICAMP), Vital Brasil, 80, Cidade Universitária "Zeferino Vaz", Campinas, SP 13083-888, Brazil. Tel/Fax: +55 19 3521 8909; E-mail: icendes@unicamp.br

Abstract

Objectives: We compared the proteomic signatures of the hippocampal lesion induced in three different animal models of mesial temporal lobe epilepsy with hippocampal sclerosis (MTLE+HS): the systemic pilocarpine model (PILO), the intracerebroventricular kainic acid model (KA), and the perforant pathway stimulation model (PPS). **Methods**: We used shotgun proteomics to analyze the proteomes and find enriched biological pathways of the dorsal and ventral dentate gyrus (DG) isolated from the hippocampi of the three animal models. We also compared the proteomes obtained in the animal models to that from the DG of patients with pharmacoresistant MTLE+HS. **Results**: We found that each animal model presents specific profiles of proteomic changes. The PILO model showed responses predominantly related to neuronal excitatory imbalance. The KA model revealed alterations mainly in synaptic activity. The PPS model displayed abnormalities in metabolism and oxidative stress. We also identified common biological pathways enriched in all three models, such as inflammation and immune response, which were also observed in tissue from patients. However, none of the models could recapitulate the profile of molecular changes observed in tissue from patients. **Significance**: Our results indicate that each model has its own set of biological responses leading to epilepsy. Thus, it seems that only using a combination of the three models may one replicate more closely the mechanisms underlying MTLE+HS as seen in patients.

INTRODUCTION

Most patients with mesial temporal lobe epilepsy (MTLE) present hippocampal sclerosis (HS), a lesion characterized by neuronal loss and gliosis, primarily in the *Cornu Ammonis* (CA) 1 and 3.[1-3] The hippocampal formation comprises CA1 to CA4, the dentate gyrus (DG), the subiculum, and the entorhinal cortex.[1,2] In rodents, the DG can be divided into dorsal and ventral portions (dDG and vDG, respectively) and posterior and anterior regions in humans. These regions present distinct cytoarchitecture with different functions.[3,4]

Surgical resection of the hippocampal formation is an established treatment for patients with pharmacoresistant MTLE, and the removed tissues can be used for further studies[5,6]; but, there are intrinsic limitations.[7] Most importantly, these specimens represent an advanced stage of the disease because they are usually obtained from patients with recurrent seizures for many years.[8,9] The use of experimental animal models of epilepsy is an alternative to overcome these limitations in searching for insights into the biological mechanism leading to disease.[10] Several rodent models have been developed, presenting characteristics like those found in patients, including a hippocampal lesion comparable to HS.[11-13] In addition, rodent models have significantly contributed to developing anti-seizure drugs in preclinical assays.[10,14,15] However, it is still unclear how similar are the molecular mechanisms leading to chronic seizures in these animals compared to patients with MTLE+HS.

Ideally, an animal model of a human disease should recapitulate the causal mechanism of the disease as seen in patients. In addition, it should present a similar phenotype and response to treatment.[16-19] Rodents have been one of the most used animal models in epilepsy research due to advantages such as the control over genetic variability, suitable lifespan, and the similar pattern of insult induction—time, intensity, and insult location.[10,14,27] Moreover, studying animal models allows for evaluating the initial stages of the disease, which is not feasible when examining human surgical tissue.[10] However, the genetic background of the animals may represent a confounding factor because variation in gene expression patterns, gene networks, and protein functions may be species-specific.[17,18,28]

Proteomics allows a broad view of the complex molecular processes in disease by assessing protein abundances in a determined disease stage.[29] In addition, cellular processes that depend on multiple genes and posttranscriptional and posttranslational modifications can be identified by proteomics.[29,30]

In the present study, we compared the proteomic profile of the granule cells isolated from the DG of three animal models of MTLE+HS: the systemic pilocarpine model (PILO), the intracerebroventricular kainic acid model (KA), and the perforant pathway stimulation model (PPS). In addition, we studied surgical tissue obtained from patients with medically refractory MTLE+HS.

The proteomic data of the PILO and PPS model used in the current study have been previously reported in detail elsewhere.[16,17] In contrast, novel data were generated for the KA model and the patients' surgical samples.

MATERIAL AND METHODS

Animals

The animal research ethics committee from the Biology Institute, University of Campinas, approved all the animal procedures described below, which were performed according to national regulations (Brazilian federal law 11.794 from 8 October 2008) and international recommendations (experiments were designed and executed following the ARRIVE guidelines and the Basel declaration including the 3R concept; www.basel-declaration.org). We used 12-week-old male Wistar rats (PILO model, $n = 5$; KA model, $n = 3$; PPS model, $n = 4$) kept under controlled conditions of 12-h light/12-h dark cycles, with lights on starting at 07:00 h. The animals had water and food available ad libitum during the experimental period.

For the induction of the PILO model, we performed a protocol described previously.[17] The KA induction was achieved using the injection of 1.25 μg of KA through a cannula under anesthesia. The animals were in *status epilepticus* (SE) for 4 h. SE was interrupted with diazepam administration (4 mg/kg), and the animals were constantly monitored using video for 15 days. The *sham* control animals were injected with saline solution instead of KA, and they also received diazepam 4 h after the first injection. PPS was performed according to a protocol reported previously.[16,18]

Animals were euthanized 15 days after the induction process described above, a period corresponding to the "latent phase." At this time, the animals still did not present spontaneous seizures, but studies have shown that the animal models display intensive molecular changes relevant to epileptogenesis.[19-21] The brains were collected and immediately frozen at −60°C with dry ice and isopentane, and the samples were stored at −80°C until further processing.

Surgical tissue from patients with medically refractory MTLE

The Research Ethics Committee of the University of Campinas approved the research protocol, and all patients

and controls provided written informed consent before entering the study. We included patients with temporal lobe epilepsy who had a clear epileptic focus localized in the mesial structures and the imaging showing signs of HS (hippocampal atrophy and hyper signal in T2/FLAIR sequences), with no other lesions associated.[22]

The presurgical clinical evaluation of patients was performed using established protocols[23-25] and was carried out by an experienced clinical team. We used hippocampal tissue isolated from patients who had undergone surgery ($n = 10$), immediately frozen with isopentane ($-60°C$) on dry ice. In addition, we selected samples from patients who had the disease for <20 years. Finally, postmortem tissue from patients without neurological disease was used as a control ($n = 4$). These hippocampal samples were collected in the same hospital with an average postmortem interval of 6–12 h (the time between death and the tissue collection). A neuropathologist examined all samples, and only samples with the classical features of mesial temporal sclerosis (pyramidal cell loss and gliosis in the CA sectors; ref PMID: 23692496) were included in the patient group. Moreover, any autopsy sample with histopathological abnormalities was excluded from the control group.

Laser microdissection procedures

Tissue samples were processed and stored under the same conditions, except that the human tissue was not subdivided (Fig. 1). For the laser microdissection, we followed the same procedures as published previously.[16,17] Once isolated, all the samples were stored at $-20°C$ until protein extraction.

Mass spectrometry and bioinformatic analyses

We used the same protocol for protein extraction, and sample preparation described previously[16,17] in three animal models, patients, and controls for protein extraction and sample preparation as described previously.[16,17] In addition, we performed a label-free liquid chromatography–tandem mass spectrometry (LC–MS/MS) as described in detail in our previous works[16,17] for the samples from PILO, KA, and PPS models. Samples from PILO and KA were analyzed at the center of toxins, immune response, and cell signaling, Butantan Institute São Paulo, Brazil; samples from the PPS model were analyzed at the Brazilian Biosciences National Laboratory, Centro Nacional de Pesquisa em Energia e Materiais, Campinas, Brazil. We analyzed the samples from patients using a Thermo Scientific™ Q Exactive™ Hybrid Quadrupole-Orbitrap Mass Spectrometer coupled with a nanoflow LC system on the front-end. This instrument was housed at the RASR Laboratory, Department of Chemistry, Vanderbilt University, Nashville, TN, USA. Injected samples were analyzed on an Ultimate 3000 RSLCnano system (Thermo Fisher Scientific, Waltham, MA, USA) coupled to a Q-Exactive operated in data dependent, positive mode. Peptides were loaded onto a C18 trap column before loading to an in-house C18 packed column, with a 105 min gradient: 0–7 min, 10% B: 7–67 min, 10–30% B: 67–75 min, 30–60% B: 75–77 min, 60–90% B: 77–82 min, 90% B: 83–105 min, 10% B. Mobile phase A was 0.1% FA in water and mobile phase B was 0.1% FA in acetonitrile. Full MS spectra were collected in the Orbitrap (375–1800 m/z, 60,000
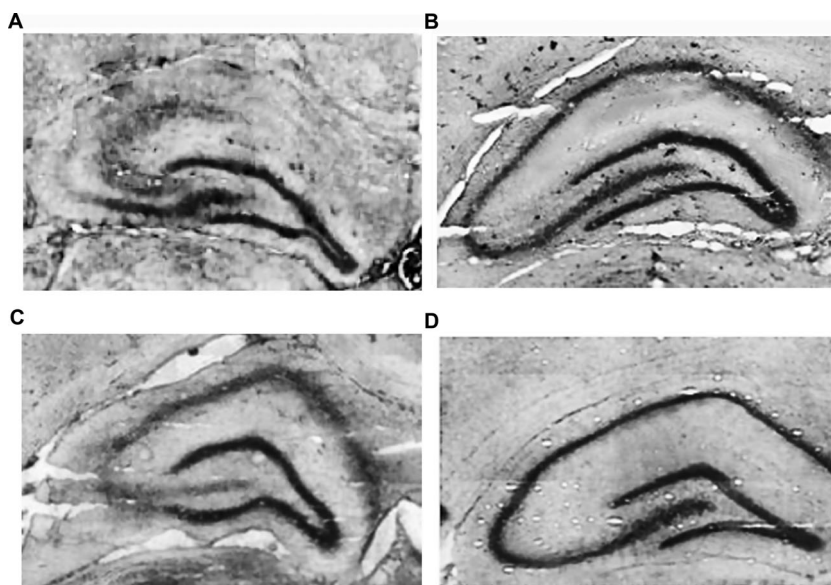
Figure 1. Image of the dorsal dentate gyrus (dDG) from the three animal models analyzed depicting the neuronal damage caused by the seizure induction. (A) The dorsal dentate gyrus of the perforant pathway stimulation (PPS-dDG) model; (B) the dorsal dentate gyrus of the pilocarpine (PILO-dDG) model; (C) the dorsal dentate gyrus of the kainic acid (KA-dDG) model, and (D) the sham control dDG.

resolution, automated gain control (AGC) 1.0E5, maximum injection time 100 msec). The instrument was operated in data-dependent acquisition mode to acquire the top 15 MS/MS (Resolution 30,000, Maximum IT 50 msec, normalized collision energy 30%, AGC 8.0E3) and dynamic exclusion of 10 sec.

We analyzed the data using Proteome Discoverer 2.4 from Thermo Fisher Scientific and R software. The database used was Uniprot for *Rattus norvegicus* (Proteome UP000002494 - downloaded on 05 January 2019–29,943 protein sequences) for the animal models and Uniprot for *Homo sapiens* (Proteome UP000005640 - downloaded on 08 November 2019–73,801 protein sequences) for the patient samples. We applied a *t*-test corrected for multiple comparisons using the Benjamini–Hochberg false discovery rate[26] at a level of 5% for each comparison. Each group of samples was analyzed separately, and we compared the epileptic animals with their respective sham controls and the patients with the autopsy controls. The final list of differentially abundant proteins for each group (animal models and patients) was used to generate the enrichment analysis.

Comparison of the proteomic profiles

We generated enrichment analysis for each model and hippocampal region using the Metacore software (Clarivate Analytics, London, UK). We also generated the enriched pathways and Gene Ontology (GO) biological processes and used qualitative analysis to compare the findings for each model and hippocampal region. In addition, we compared the complete list of proteins to identify the number of shared proteins among the three different animal models and to which protein classes they belong.

To compare the animal models and the human tissue, we also used qualitative analysis to identify common biological responses generated with the enriched pathways and GO biological processes. To evaluate common proteins among all models and patient tissue, we first mapped the rat protein IDs to gene IDs. Subsequently, we converted the rat gene IDs to human homology gene IDs using the BioMart tool from Ensembl in the R environment. Using these converted IDs, we also performed a principal component analysis (PCA) to reduce the dimensionality of the data, using singular value decomposition to examine the grouping of the samples.

RESULTS

In the dDG of the PILO model, we identified 756 proteins; 97 were differentially abundant; namely, 51 upregulated and 46 downregulated. In the vDG of the PILO model, we identified 708 proteins; 56 were differentially abundant, including 28 upregulated and 28 downregulated.[17] In the dDG of the KA model, we identified 1701 proteins, 119 differentially abundant, 73 upregulated, and 46 downregulated. In the vDG of the KA, we identified 424 proteins, 32 differentially abundant, 17 upregulated, and 15 downregulated. In the dDG of the PPS model, we identified 959 proteins, 58 differentially abundant, 26 upregulated, and 32 downregulated. Finally, in the vDG of the PPS model, we identified 898 proteins, 75 differentially abundant, with 23 upregulated and 52 downregulated.[16]

We compared the total number of proteins identified in each model using upset plots (Fig. 2A). There were 132 proteins identified solely in the dDG of the PILO model, 969 proteins only in the dDG of the KA model, and 624 proteins that were exclusively detected in the dDG of the PPS model. Comparing the PILO and KA models, we identified 404 proteins in common. In the comparison between the PILO and PPS models, we found only seven proteins in common. The comparison between the KA and PPS models revealed 116 proteins in common in the dDG. Furthermore, we found that in the dDG, there were 212 altered proteins in common in all three animal models.

In the vDG, there were 334 proteins identified only in the vDG of the PILO model, 103 in the KA model, and 693 in the PPS model (Fig. 2B). We found 182 proteins in common comparing the PILO and KA models, 66 proteins in common between the PILO and PPS models, and 14 proteins equally identified in the KA and PPS models. Moreover, there were 125 altered proteins in common in the vDG of all three animal models.

GO and enrichment analysis

To analyze the biological processes altered in each model based on the abnormal protein expression profiles, we first generated a list of GO biological processes using the differentially abundant proteins classified into nine categories (Table S1). For the PILO-dDG, the main biological processes were cellular processes (17 specific processes), inflammation (14), cellular components (9), transport (6), and neurogenesis (4). In the PILO-vDG, the major GO processes were transport (7), cellular components (4), mitochondrial processes (4), inflammation (3), neurogenesis (3), and metabolism (2). In the KA-dDG, the main GO processes were cellular processes (17), synaptic processes (10), neurogenesis (9), cellular components (8), transport (3), and inflammation (1). In the KA-vDG, we found synaptic processes (8), inflammation (7), cellular components (6), cell-cycle (5), transport (3), metabolism (3), mitochondrial processes (2), and neurogenesis (1). In

A

B
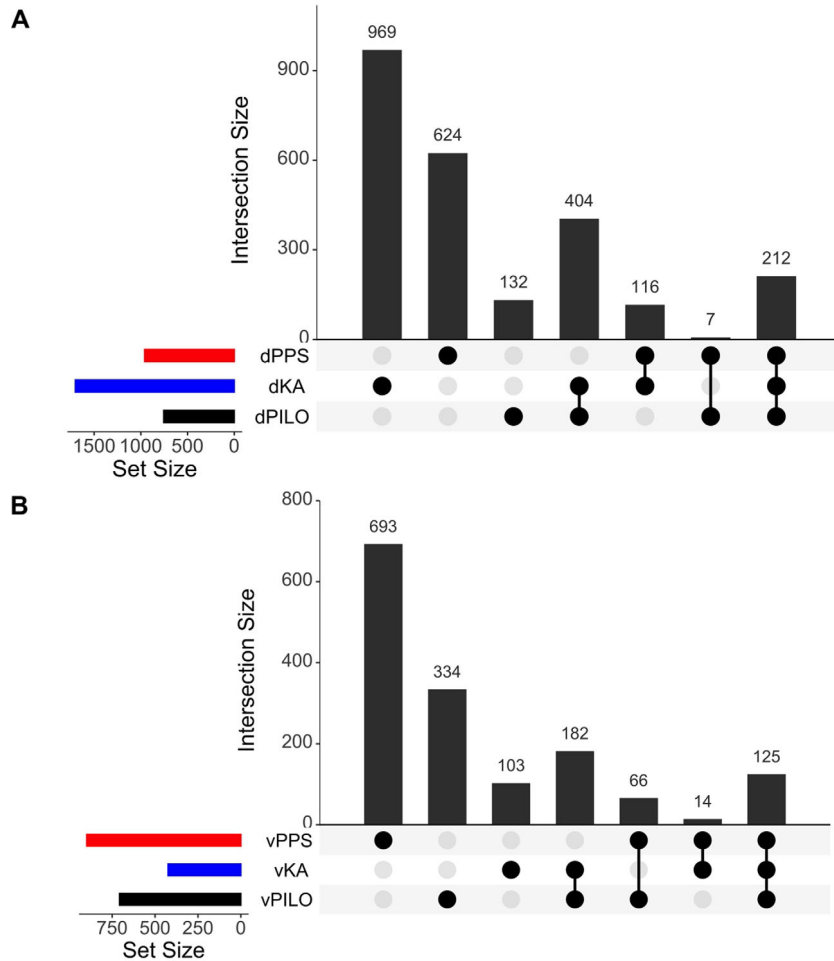
Figure 2. Upset plots with the total number of proteins identified in the three animal models of mesial temporal lobe epilepsy (MTLE). (A) The total number of proteins identified in the **dorsal dentate gyrus** from each model. dPILO, dorsal dentate gyrus of the pilocarpine model; dKA, dorsal dentate gyrus from the kainic acid model; dPPS, dorsal dentate gyrus of the perforant pathway stimulation model. (B) The total number of proteins identified in the **ventral dentate gyrus** from each model. vPILO, ventral dentate gyrus of the pilocarpine model; vKA, ventral dentate gyrus from the kainic acid model; vPPS, ventral dentate gyrus of the perforant pathway stimulation model.

the PPS-dDG, the most represented GO processes were metabolism (17), mitochondrial processes (15), cellular processes (8), synaptic processes (5), neurogenesis (2), and transport (2). In the PPS-vDG, the GO categories were mitochondrial processes (10), cellular components (9), apoptosis (6), cellular processes (2), transport (2), and inflammation (2). In addition, we found that comparing the PILO-dDG with the KA-dDG, there were 23 GO processes in common, while the PPS-dDG did not have any GO processes in common with the dDG of the other two models. The PILO-vDG and the PPS-vDG had five GO processes in common, the PPS-vDG and the KA-vDG had seven, and the PILO-vDG and KA-vDG had 10 GO processes in common (Fig. 3).

We also analyzed the enriched pathways for each model and DG region using the list of differentially abundant proteins. Then, we classified the enriched pathways into 14 categories (Fig. 4; for a complete list of enriched pathways, refer to Table S2). The five main categories represented in the PILO-dDG were cellular processes (15 enriched pathways), development (9), stem cell (5),

cytoskeleton (4), and immune response (3). In the PILO-vDG, they were cellular processes (17), development (7), immune response (4), transcription/translation (4), and stem cell (3). In the KA-dDG, we identified immune response (13), cellular processes (8), development (8), cytoskeleton (4), and neurophysiological processes (3). The enriched pathways in the KA-vDG were cellular processes (13), development (7), cytoskeleton (4), neurophysiological processes (4), and transcription/translation (4). In the PPS-dDG, we found metabolism (11), development (10), cellular processes (8), immune response (4), neurophysiological processes (4), and transcription/translation (2). Finally, in the PPS-vDG, we found immune response (10), development (9), neurophysiological processes (6), cellular processes (5), and metabolism (4).

Human tissue

Table 1 shows the characteristics of the patients included in the study and those who donated autopsy material. We identified a total of 5140 proteins in the surgical

GO biological processes
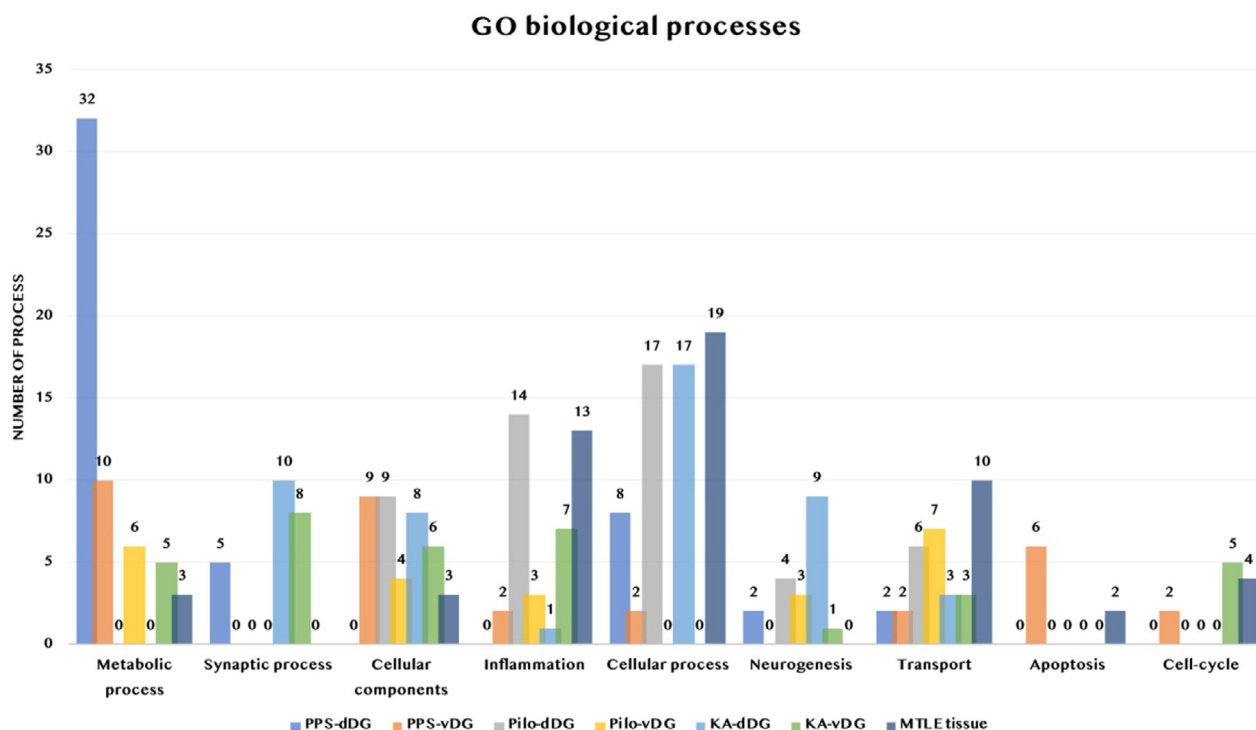
Figure 3. Gene Ontology (GO) biological processes identified from each model are divided into categories. The gray bars represent the processes observed in the pilocarpine dorsal dentate gyrus (PILO-dDG), the yellow bars represent the data from the ventral dentate gyrus from the pilocarpine model (PILO-vDG), the light blue bars represent the processes identified in the dorsal dentate gyrus of the kainic acid (KA-dDG), the green bars mark the processes seen in the ventral dentate gyrus of the kainic acid (KA-vDG), the dark blue bars represent the processes of the dorsal dentate gyrus perforant pathway stimulation (PPS-dDG), the orange bars indicate the processes of the ventral dentate gyrus perforant pathway stimulation model (PPS-vDG), and the dark blue bars show the processes of tissues from patients with mesial temporal lobe epilepsy (MTLE). The numbers above the bars show the number of processes identified in each category.

specimens of patients with medically refractory MTLE+HS; 180 were differentially abundant compared with autopsy controls, 88 upregulated and 92 downregulated. Comparing the total number of proteins identified in patients, classified by gene homology, with the number identified in each of the animal models, we found 37 proteins in common with the PILO model, 360 proteins in common with the KA model, and 277 in common with the PSS model (Fig. 5A). Figure 5B shows the top 20 proteins (represented by their genes and fold-change values) common among all three animal models and patients.

The analysis of enriched GO processes in tissue from patients revealed that the most enriched processed were cellular processes (19), inflammation (13), transport (10), signaling (5), and cytoskeleton (5); for a complete list, refer to Table S3. Comparing the GO processes identified in patients to the three models, we found that the PILO model had 42 processes in common with human data, the KA had 33, and the PPS had only two.

Moreover, the most enriched pathways found in tissue from patients were cellular processes (15), development (7), neurophysiological processes (5), signal transduction

(5), and cytoskeleton (5) (Table S3). Comparing the enriched pathways identified in the human data with the three animal models, we found that the PILO model had nine enriched pathways in common with patients, the KA had seven, and the PPS model had four enriched pathways in common with the human data.

Finally, the PCA results revealed that the samples from the PILO model tended to cluster with the samples from the dDG of the KA model and the dDG of the PPS model. By contrast, the patient samples were independent of all other groups (Fig. 6).

DISCUSSION

This study first evaluated proteins individually; we determined the number of proteins identified and their relative abundance compared with controls. We subsequently grouped proteins in classes by performing enrichment analyses to assess the most relevant biological processes in each epilepsy animal model and human tissue.[31] Furthermore, we analyzed the enriched pathways, which provided an overview of the biological cascades and molecular interactions activated.[32]
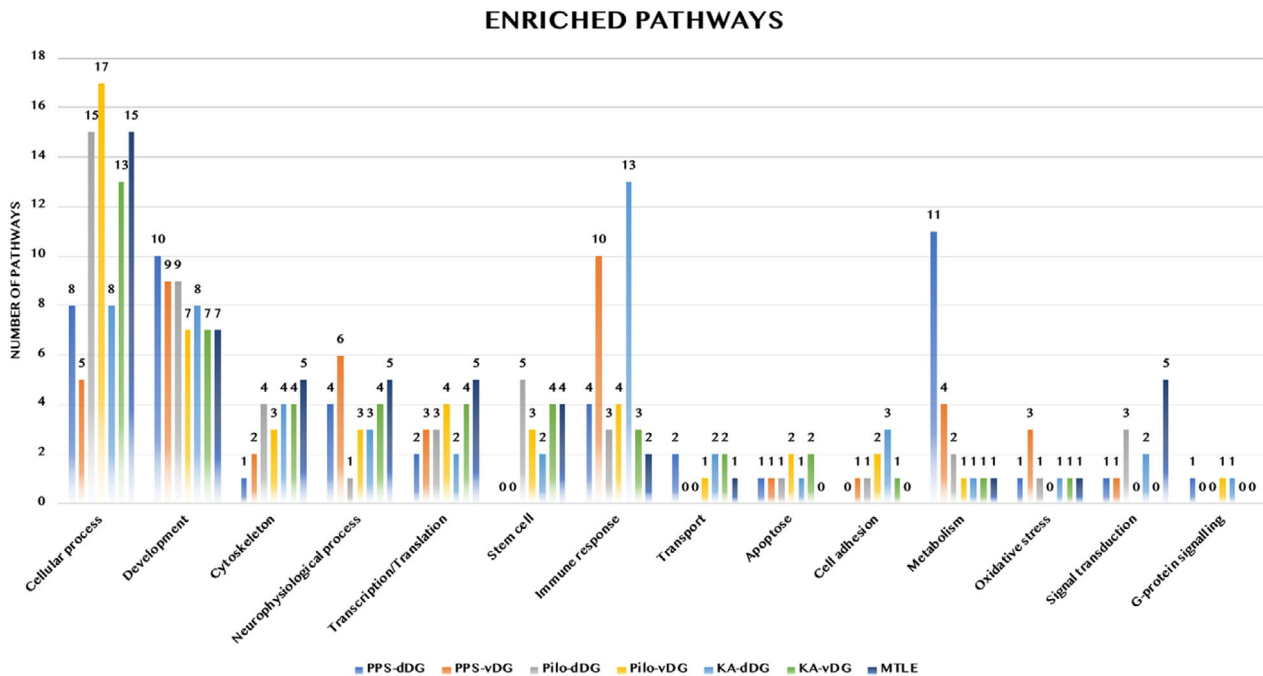
ENRICHED PATHWAYS

Figure 4. Enriched pathways identified for each model are divided into categories. The gray bars represent the pathways of the dorsal dentate gyrus of the pilocarpine model (PILO-dDG), the yellow bars represent the ventral dentate gyrus of the pilocarpine model (PILO-vDG), the light blue bars represent the pathways identified in the dorsal dentate gyrus of the kainic acid model (KA-dDG), the green bars show the pathways of the ventral dentate gyrus of the kainic acid model (KA-vDG), the light blue bars represent the pathways of the dorsal dentate gyrus of the perforant pathway stimulation model (PPS-dDG), the orange bars indicate the pathways of the ventral dentate gyrus of the perforant pathway stimulation model (PPS-vDG), and the dark blue bars represent the pathways from tissues of patients with mesial temporal lobe epilepsy (MTLE). Numbers above the bars show the number of enriched pathways identified in each category.

The PILO model uses a chemoconvulsant, pilocarpine, which acts as an agonist of the cholinergic muscarinic receptors, inducing prolonged epileptic activity resulting in SE.[20,33] The KA model also uses a chemical compound, KA, an L-glutamate cyclic analog that induces a prolonged excitatory response in the neurons resulting in SE. The intracerebroventricular administration of KA results in behavior similar to systemic pilocarpine induction.[19,34] By contrast, the PPS model is induced by consecutive electrical stimulations restricted to the perforant pathway; this stimulation does not generate a phenotypically recognizable SE but results in hippocampal damage that resembles human HS. It also produces spontaneous epileptiform discharges in the granule cells of the hippocampus preceding the spontaneous seizure phenotype.[21] Animal models presenting SE mimic an early precipitating brain insult, which occurs before spontaneous seizures start, and when it is believed that most of the molecular changes leading to epilepsy develop.[7,35]

Proteomic profile of the KA model

We found significant abnormalities in the synaptic processes identified in both the dDG and the vDG of the KA

model. The main processes involved are presynaptic endocytosis, synaptic vesicle recycling, vesicle-mediated transport in the synapse, regulation of synapse structure or activity, and synaptic vesicle budding (for a complete list, refer to Tables S1, S2). Increased synaptic activity has been observed in the KA model, a phenomenon that can result from the overstimulation of the glutamatergic system and may be related to the presence of an excitatory imbalance.[36,37]

Furthermore, we found two other relevant biological mechanisms altered in the KA model, namely cytoskeletal remodeling and neurogenesis. The main abnormal processes and pathways enriched in the dDG and the vDG of the KA model were Hyaluronic acid/CD44 signaling pathways, neurofilaments, generation of neurons, axonogenesis, and regulation of neuronal projection development. Granule cells are the primary constituent cell type of the DG, and it is one of the few types that may undergo neurogenesis throughout adult life.[3]

To our knowledge, there have been only two other studies reporting MS-based proteomics data in the KA model of epilepsy. One report describing the proteomic profile of the whole hippocampus in a mouse KA model evaluated in three time points.[38] They observed, especially

Table 1. Characteristics of patients with mesial temporal lobe epilepsy included in this study, as well as autopsy controls.

Subject	Age	Disease duration[1]	Sex	Surgical outcome[2]	Neuroimage	Type of HS[3]
1	20	19	F	Responsive IIa	LHA	1
2	27	15	M	Responsive Ia	Bilateral HA, prevalent in the left hippocampus	1
3	46	17	M	Responsive Ia	RHA	1
4	18	17	M	Responsive Ia	RHA	1
5	47	20	F	Responsive Ia	LHA	1
6	36	19	F	Responsive Ia	LHA	1
7	22	4	F	Refractory IIIa	RHA	1
8	31	19	M	Responsive Id	RHA	1
9	33	16	M	Responsive IIa	LHA	1
10	26	19	F	Responsive Ia	LHA	1

Control	Age	–	Sex	Cause of death	–	–
1	55	–	F	Acute pulmonary thromboembolism	NA	–
2	66	–	F	Septic shock	NA	–
3	54	–	M	Septic shock, pneumonia, tubular necrosis	NA	–
4	56	–	F	Cryptogenic cirrhosis	NA	–

All patients had alterations in images obtained by magnetic resonance compatible with hippocampal atrophy, namely decreased hippocampal volume in T1 images with increased signal in T2/FLAIR. All findings were confirmed by histopathological evaluation after surgery. HS, hippocampal sclerosis; HA, hippocampal atrophy; LHA, hippocampal atrophy in the left hippocampus; RHA, hippocampal atrophy in the right hippocampus; NA, not available; ILAE, International League Against Epilepsy.
[1]Disease duration is calculated as the time between the first seizure and epilepsy surgery.
[2]Surgical outcome was defined based on the Commission on Neurosurgery of the ILAE.[21]
[3]As seen in the neuropathology.

at the 30-day time point, decreased expression of proteins related to neuroplasticity and axonal regeneration.[38] Another study used proteomics to evaluate the posttranslational modifications of sodium channels and found evidence of phosphorylation and methylation of these channels after seizures.[39] Thus, our results expand these previous findings and show regional differences in the proteomics profile of the dDG and the vDG in the KA model.

Proteomic profile of the patient tissue

For this study, we generated the proteomic profile of microdissected granule cells of the DG of 10 patients with pharmacoresistant MTLE+HS who had surgical treatment. On the average, epilepsy surgery was performed 16 years after the onset of chronic seizures. Thus, the time point in which we obtained the tissue from patients is different from that of the animal models.

We found significant abnormalities in inflammation and immune response biological pathways in tissue from patients with MTLE+HS. The main processes we identified were myeloid cell activation involved in immune response, myeloid leukocyte-mediated immunity, neutrophil activation involved in the immune response, and cell activation involved in the immune response. Inflammatory pathways are among the most common molecular mechanisms found in epilepsy studies; they may contribute to the disease development and progression.[40] Neurogenic inflammation is an inflammatory response triggered by exacerbated neuronal activity without other pathological conditions, such as infections. Neuroinflammation may affect neuronal activity directly or indirectly by mediating other molecules and cells, such as the physiology of astrocytes.[40,41] Overall, these effects would contribute to increased excitability, altered neurotransmission, and epilepsy-induced neuropathological changes.[41]

Figure 5. Gene homology analysis of the total number of proteins identified in the three animal models and patients with mesial temporal lobe epilepsy (MTLE). (A) Upset plot of the total number of proteins identified in the three animal models and patients. PILO, Pilocarpine model; KA, kainic acid model; PPS, perforant pathway stimulation model; MTLE, patients with mesial temporal lobe epilepsy. (B) List of the the top 20 genes in common among the four groups analyzed and their log2 fold-change illustrating the abundancy variation in each group. dPILO, dorsal dentate gyrus from the pilocarpine model; vPILO, ventral dentate gyrus of the pilocarpine model; dKA, dorsal dentate gyrus of the kainic acid model; vKA, ventral dentate gyrus of the kainic acid model; dPPS, dorsal dentate gyrus of the perforant pathway stimulation model; vPPS, ventral dentate gyrus of the perforant pathway stimulation model.
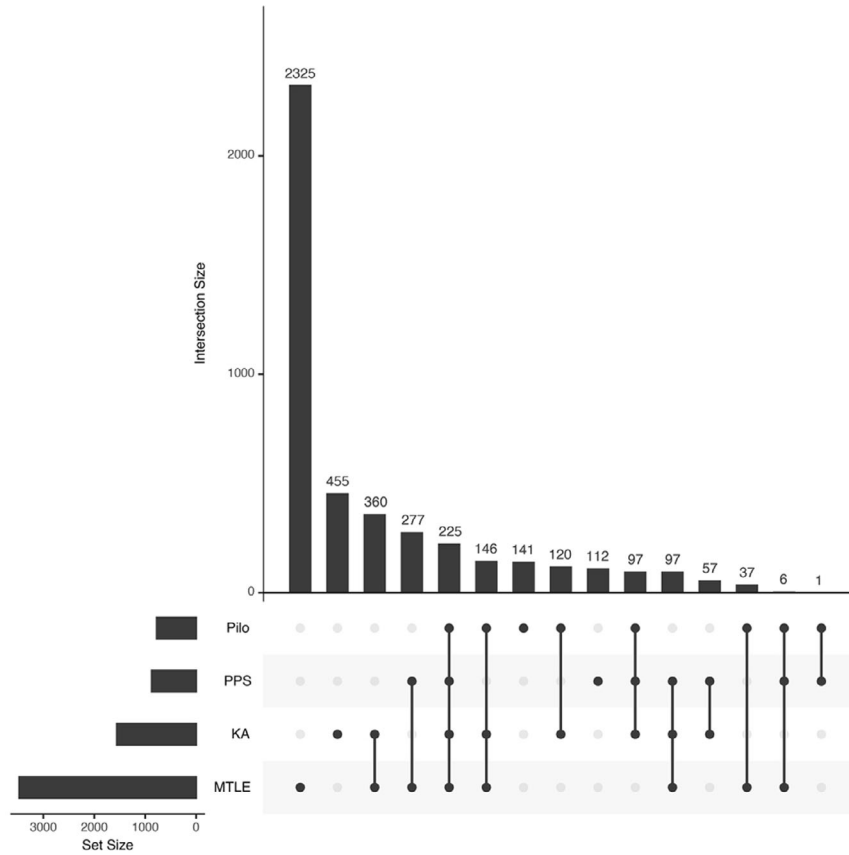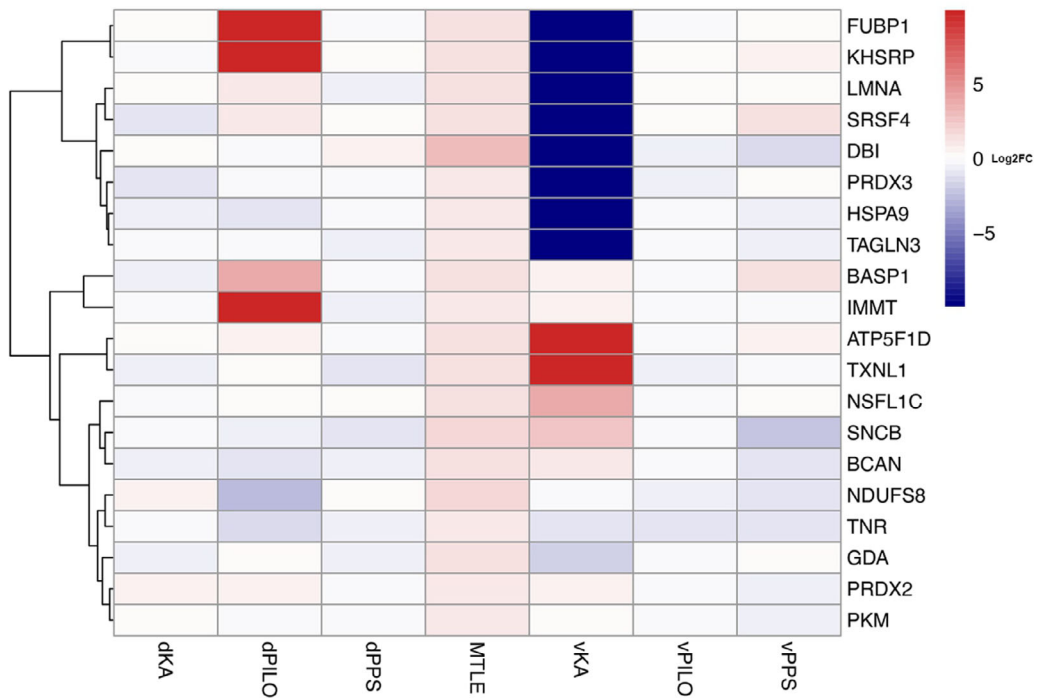
Figure 6. Principal component analysis (PCA) generated with the homologous human gene IDs converted from rats to humans (for the animal models) using the BioMart tool. The chart shows the distribution of the models and patients with mesial temporal lobe epilepsy (MTLE), according to their log2 fold-change values and human gene IDs. PILO, Pilocarpine model; KA, kainic acid model; PPS, perforant pathway stimulation model; MTLE, patients with mesial temporal lobe epilepsy.
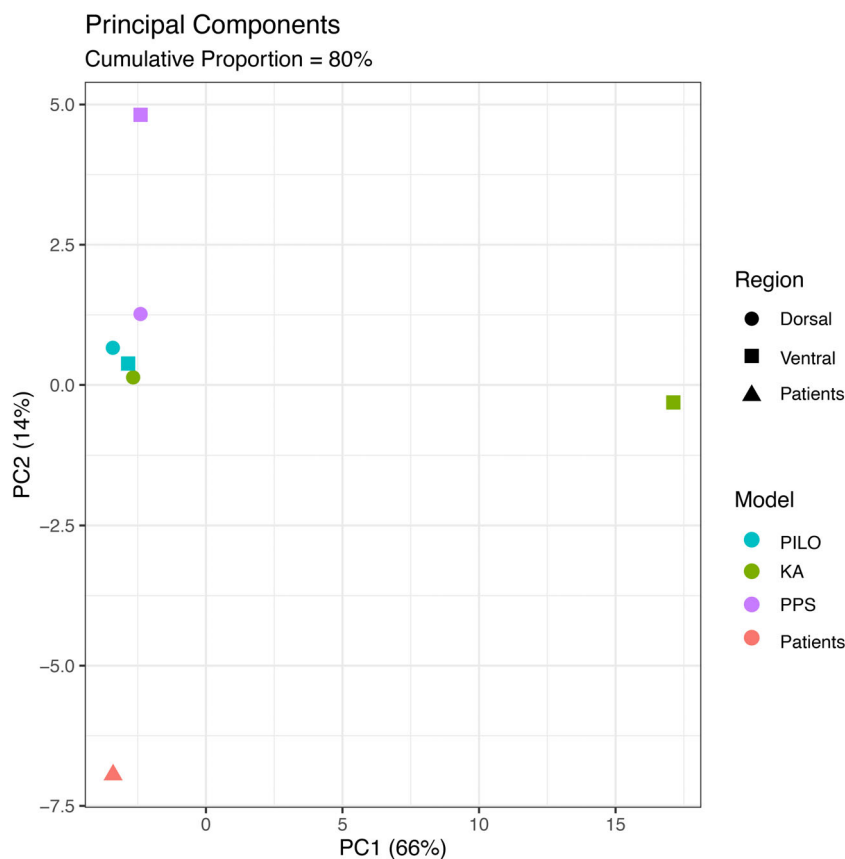
We also found other important biological mechanisms altered in tissue from patients, including cytoskeletal remodeling (cytoskeleton organization, cytoskeleton keratin filaments, neurofilaments, regulation of actin cytoskeleton nucleation, and polymerization by Rho GTPases) and metabolism (activation of NOX1, NOX5, and DUOX1 and DUOX2 NADPH oxidases; regulation of phosphate metabolic process; regulation of phosphorus metabolic process; and regulation of catalytic activity), mainly related to oxidative stress, and changes in several signaling processes (putative ubiquitin pathway, regulated exocytosis, secretion, and regulation of ion transport, among others) (Table S3). Metabolic changes, especially oxidative stress, are frequent in epilepsy, resulting from the overproduction of reactive oxygen and reactive nitrogen species.[41] Oxidative stress is rapidly induced in the nervous system by acute injuries, including SE.[41,42] This response is known to involve neurons and glia and is highly connected with inflammatory responses.[44]

In addition, there were abnormalities in neurophysiological processes such as glutamic acid regulation of dopamine D1A receptor signaling, constitutive and regulated NMDA receptor trafficking, and delta-type opioid receptors in the nervous system. Dopamine is an amine neuromodulator synthesized in the brain and kidneys,[28] and its modulation seems to be involved in seizures in the limbic system.[43] Its receptors are expressed mainly in the DG and subventricular zone in the central nervous system, and evidence has shown that the dopamine receptor D1 is pro-epileptogenic.[43] Moreover, the effects of dopamine seem to be related to the glutamate–dopamine interaction.[43,44]

We also identified enriched high-density lipoprotein pathways (HDL)-mediated reverse cholesterol transport and HDL dyslipidemia in type 2 diabetes and metabolic syndrome X in tissue from patients. Cholesterol is synthesized locally in the brain, and this process is decreased after neuronal damage, increasing cholesterol uptake from degenerating synaptic terminals.[45,46] Interestingly, alterations in cholesterol metabolism have already been reported in the PILO and PPS models.[18,45]

Comparing the proteomic profile in the different animal models

We found differences in the abundance of proteins when comparing the three animal models (PILO, KA, and PPS). Furthermore, as we have shown previously, there

Abundancy pattern %
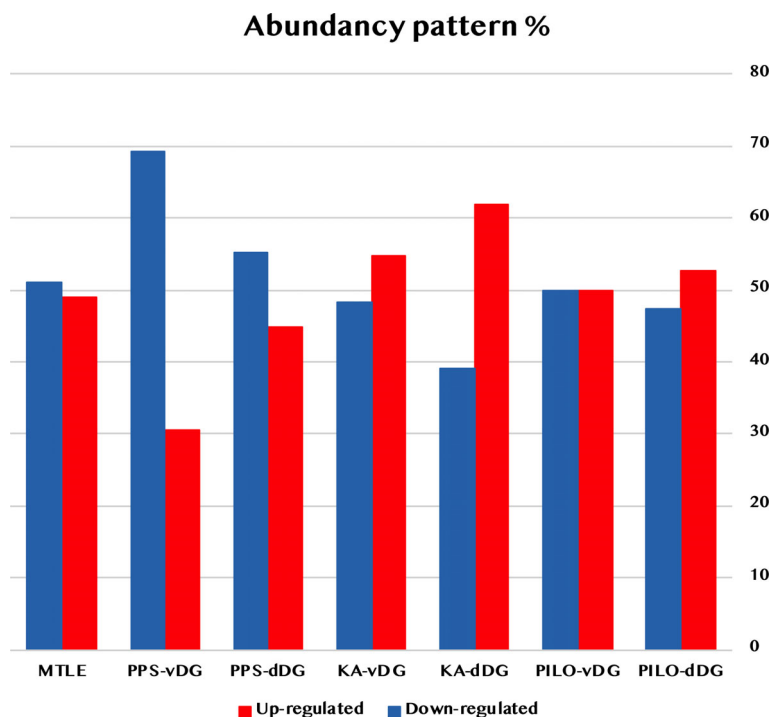
Figure 7. Differentially abundant proteins were identified in each model and hippocampal region and the tissue from patients. The graph shows the percentage of upregulated and downregulated proteins. Blue bars represent the upregulated proteins, and red bars represent the downregulated proteins. PILO-dDG, dorsal dentate gyrus of the pilocarpine model; PILO-vDG, ventral dentate gyrus of the pilocarpine model; KA-dDG, dorsal dentate gyrus of the kainic acid model; KA-vDG, ventral dentate gyrus of the kainic acid model; PPS-dDG, dorsal dentate gyrus of the perforant pathway stimulation model; PPS-vDG, ventral dentate gyrus of the perforant pathway stimulation model.

were differences in protein abundances when comparing the dorsal and ventral portions of the DG in the same animal model[20,21] (Fig. 7). However, there were also differentially abundant proteins in common among the three animal models. There were more similarities between the PILO and KA models (404 proteins in the dDG and 182 in the vDG) than between the PILO and PPS models (7 proteins in the dDG and 66 in the vDG) or between the KA and PPS models (116 proteins in the dDG and 14 in the vDG). One may expect the PILO and KA models to be more closely related because, in both, a chemical compound activates biological mechanisms that converge on excitatory response to induce SE.

Based on the proteomic signature, we found that the PILO and KA models predominantly involved the following GO processes: inflammation, cellular components, and neurogenesis. The most enriched cellular processes in common observed in the PILO and KA were cytoskeleton, stem cell-related pathways, and cell adhesion (Figs. 3, 4). Comparing the PILO and PPS models did not result in processes and pathways exclusive to the two models. However, the KA and PPS models shared molecular alterations related to synaptic activity and cell-cycle, even though these alterations were more significant in the KA model (Figs. 3, 4). Of note, there were highly enriched biological processes and pathways specific to the PPS-vDG, all related to apoptosis: Regulation of neuron death, regulation of neuron apoptotic process, regulation of the apoptotic process, and regulation of programmed cell death.

Most importantly, we identified abnormalities that were common to all three animal models. These were GO processes and pathways involving cellular processes and components, mainly intracellular transport, cell localization, protein assembly, protein localization, and cell morphogenesis. We hypothesize that these may result from the stimuli used to induce the models, which generates a common cell response because external stimuli trigger a series of stereotypical reactions in neuronal cells.[31,46] We also found highly enriched pathways related to development in all regions and models (Fig. 4 and Table S2). The main abnormal pathways were NCAM1-mediated neurite outgrowth, synapse assembly, and neuronal survival (PILO-dDG); The role of CDK5 in neuronal development (PILO-vDG); S1P2 and S1P3 receptors in cell proliferation and differentiation (KA-dDG); Glucocorticoid receptor signaling (KA-vDG); WNT signaling pathway (PPS-dDG); and transactivation of PDGFR in non-neuronal cells by dopamine D2 receptor (PPS-vDG). Interestingly, these enriched pathways related to developmental processes did not appear in the analysis of enriched GO processes (Fig. 3), emphasizing the complementary nature of the two assessments.

However, considering that the models studied here are induced by different methods, one can expect some biological differences, especially the timing to which molecular changes may occur. This is an important issue in the present work since we analyzed the animal models at the same time point. Given that studies employing omics tools to describe detailed time-specific molecular changes are not

available in the literature for the three models, the 15 days after induction time-point was chosen based on the average duration of the "silent period" for the different models compared in the present study: 24 days for the PILO model, 7 to 14 days for the KA model, and 21 days for the PPS model.[47,48] Thus, the 15 days after induction consists of the longest possible interval after the initial insult that would not enter the period of spontaneous seizures. Therefore, although based on the best knowledge available in the literature, we cannot completely exclude the possibility that the changes found in our study represent, at least in part, differences in the kinetics of activation of each pathway in the different animal models.

Comparing animal models and patient tissue

As shown by the PCA analysis (Fig. 6), the proteomic profile obtained in patients was different from the three animal models. However, there were some features in common. Indeed, each animal model seems to recapitulate different molecular aspects seen in patients. The PILO model seems to represent better the neurophysiological processes, the KA model shows the abnormal synaptic activity, and the PPS model resembles the abnormal metabolic processes observed in the tissue of patients with MTLE+HS. Furthermore, we found exacerbated inflammation and immune response in all groups studied.

Overall, our results indicate that each model has its own set of biological responses, leading to epilepsy. However, there are common biological pathways enriched in all three models, such as inflammation and immune response, which are also present in tissue from patients with MTLE+HS. Given the differences we identified among the animal models, it seems that only using a combination of the three models may one replicate more closely the mechanisms underlying MTLE+HS as seen in patients.

Acknowledgments

Conflict of Interest

The authors declare no conflict of interest related to the present work.

Author Contributions

(1) Conception and design of study - Amanda M. Canto, Andre S. Vieira, Fernando Cendes, and Iscia Lopes-Cendes. (2) Acquisition and analysis of data - Amanda M. Canto, Alexandre B. Godoi, Alexandre H. B. Matos, Jaqueline C. Geraldis, Fabio Rogerio, Marina K. M. Alvim, Clarissa L. Yasuda, Enrico Ghizoni, Helder Tedeschi, Diogo F. T. Veiga, Barbara Henning, Welliton Souza, Cristiane S. Rocha, Andre S. Vieira, Elayne V. Dias, Benilton S. Carvalho, Rovilson Gilioli, Albert B. Arul, and Renã A. S. Robinson. (3) Drafting a significant portion of the manuscript or figures - Amanda M. Canto, Alexandre B. Godoi, Diogo F. T. Veiga, Welliton Souza, Benilton S. Carvalho, and Iscia Lopes-Cendes.

REFERENCES

1. Amaral DG, Witter MP. The three-dimensional organization of the hippocampal formation: a review of anatomical data. Neuroscience. 1989;31(3):571-591.
2. Blümcke I, Thom M, Aronica E, et al. International consensus classification of hippocampal sclerosis in temporal lobe epilepsy: a task force report from the ILAE commission on diagnostic methods. Epilepsia. 2013;54:1315-1329.
3. Amaral DG, Scharfman HE, Lavenex P. The dentate gyrus: fundamental neuroanatomical organization (dentate gyrus for dummies). Prog Brain Res. 2007;163:3-22.
4. Jonas P, Lisman J. Structure, function, and plasticity of hippocampal dentate gyrus microcircuits. Front Neural Circuits. 2014;8. doi:10.3389/fncir.2014.00107/abstract
5. Wiebe S, Blume WT, Girvin JP, Eliasziw M. Effectiveness and efficiency of surgery for temporal lobe epilepsy study group. A randomized, controlled trial of surgery for temporal-lobe epilepsy. N Engl J Med. 2001;345(5):311-318.
6. Boling W. Surgical considerations of intractable mesial temporal lobe epilepsy. Brain Sci. 2018;8(2):35.
7. Pitkänen A, Lukasiuk K, Dudek FE, Staley KJ. Epileptogenesis. Cold Spring Harb Perspect Med. 2015;5(10):a022822.
8. Rakhade SN, Jensen FE. Epileptogenesis in the immature brain: emerging mechanisms. Nat Rev Neurol. 2009;5(7):380-391.
9. Pitkänen A, Engel J. Past and present definitions of epileptogenesis and its biomarkers. Neurotherapeutics. 2014;11(2):231-241.
10. Becker AJ. Review: animal models of acquired epilepsy: insights into mechanisms of human epileptogenesis. Neuropathol Appl Neurobiol. 2018;44(1):112-129.
11. Avanzini G, Vergnes M, Spreafico R, Marescaux C. Calcium-dependent regulation of genetically determined spike and waves by the reticular thalamic nucleus of rats. Epilepsia. 1993;34(1):1-7.

12. Engel J. Excitation and inhibition in epilepsy. Can J Neurol Sci. 1996;23(3):167-174.

13. Isokawa M. Preservation of dendrites with the presence of reorganized mossy fiber collaterals in hippocampal dentate granule cells in patients with temporal lobe epilepsy. Brain Res. 1997;744(2):339-343.

14. Grone BP, Baraban SC. Animal models in epilepsy research: legacies and new directions. Nat Neurosci. 2015;18(3):339-343.

15. Barker-Haliski ML, Friedman D, French JA, White HS. Disease modification in epilepsy: from animal models to clinical applications. Drugs. 2015;75(7):749-767.

16. do Canto AM, Vieira AS, H B Matos A, et al. Laser microdissection-based microproteomics of the hippocampus of a rat epilepsy model reveals regional differences in protein abundances. Sci Rep. 2020;10 (1):4412.

17. Canto AM, Matos AHB, Godoi AB, et al. Multi-omics analysis suggests enhanced epileptogenesis in the *Cornu Ammonis* 3 of the pilocarpine model of mesial temporal lobe epilepsy. Hippocampus. 2021;31(2):122-139.

18. Vieira AS, de Matos AH, do Canto AM, et al. RNA sequencing reveals region-specific molecular mechanisms associated with epileptogenesis in a model of classical hippocampal sclerosis. Sci Rep. 2016;6:22416.

19. Williams PA, White AM, Clark S, et al. Development of spontaneous recurrent seizures after kainate-induced status epilepticus. J Neurosci. 2009;29(7):2103-2112.

20. Cavalheiro EA, Leite JP, Bortolotto ZA, Turski WA, Ikonomidou C, Turski L. Long-term effects of pilocarpine in rats: structural damage of the brain triggers kindling and spontaneous recurrent seizures. Epilepsia. 1991;32 (6):778-782.

21. Norwood BA, Bumanglag AV, Osculati F, et al. Classic hippocampal sclerosis and hippocampal-onset epilepsy produced by a single "cryptic" episode of focal hippocampal excitation in awake rats. J Comp Neurol. 2010;518(16):3381-3407.

22. Cendes F, Sakamoto AC, Spreafico R, Bingaman W, Becker AJ. Epilepsies associated with hippocampal sclerosis. Acta Neuropathol. 2014;128(1):21-37.

23. Kwan P, Arzimanoglou A, Berg AT, et al. Definition of drug resistant epilepsy: consensus proposal by the ad hoc task force of the ILAE commission on therapeutic strategies. Epilepsia. 2010;51(6):1069-1077.

24. de Souza JPSAS, Ayub G, Nogueira M, et al. Temporopolar amygdalohippocampectomy: seizure control and postoperative outcomes. J Neurosurg. 2020;134 (3):1044-1053.

25. Mota MVB, Zaidan BC, do Canto AM, et al. ATP synthase subunit Beta immunostaining is reduced in the sclerotic hippocampus of epilepsy patients. Cell Mol Neurobiol. 2019;39(1):149-160.

26. Avansini SH, Torres FR, Vieira AS, et al. Dysregulation of *NEUROG2* plays a key role in focal cortical dysplasia: *NEUROG2* dysregulation in FCD. Ann Neurol. 2018;83 (3):623-635.

27. Glickman ME, Rao SR, Schultz MR. False discovery rate control is a recommended alternative to Bonferroni-type adjustments in health studies. J Clin Epidemiol. 2014;67 (8):850-857.

28. Löscher W. Animal models of seizures and epilepsy: past, present, and future role for the discovery of antiseizure drugs. Neurochem Res. 2017;42(7):1873-1888.

29. Bhatia A, Lenchner JR, Saadabadi A. Biochemistry, dopamine receptors. StatPearls. StatPearls Publishing; 2021.

30. Zhang Z, Wu S, Stenoien DL, Paša-Tolić L. High-throughput proteomics. Annu Rev Anal Chem (Palo Alto Calif). 2014;7:427-454.

31. Li X, Wang W, Chen J. Recent progress in mass spectrometry proteomics for biomedical research. Sci China Life Sci. 2017;60(10):1093-1113.

32. Ashburner M, Ball CA, Blake JA, et al. Gene ontology: tool for the unification of biology. Nat Genet. 2000;25 (1):25-29.

33. Cary MP, Bader GD, Sander C. Pathway information for systems biology. FEBS Lett. 2005;579(8):1815-1820.

34. Curia G, Longo D, Biagini G, Jones RSG, Avoli M. The pilocarpine model of temporal lobe epilepsy. J Neurosci Methods. 2008;172(2):143-157.

35. Lévesque M, Avoli M. The kainic acid model of temporal lobe epilepsy. Neurosci Biobehav Rev. 2013;37(10):2887-2899.

36. Fisher RS, Acevedo C, Arzimanoglou A, et al. ILAE official report: a practical clinical definition of epilepsy. Epilepsia. 2014;55(4):475-482.

37. Staley K. Molecular mechanisms of epilepsy. Nat Neurosci. 2015;18(3):367-372.

38. Lau A, Tymianski M. Glutamate receptors, neurotoxicity and neurodegeneration. Pflugers Arch. 2010;460(2):525-542.

39. Bitsika V, Duveau V, Simon-Areces J, et al. High-throughput LC–MS/MS proteomic analysis of a mouse model of mesiotemporal lobe epilepsy predicts microglial activation underlying disease development. J Proteome Res. 2016;15(5):1546-1562.

40. Baek J-H, Rubinstein M, Scheuer T, Trimmer JS. Reciprocal changes in phosphorylation and methylation of mammalian brain sodium channels in response to seizures. J Biol Chem. 2014;289(22):15363-15373.

41. Vezzani A, French J, Bartfai T, Baram TZ. The role of inflammation in epilepsy. Nat Rev Neurol. 2011;7(1):31-40.

42. Terrone G, Balosso S, Pauletti A, Ravizza T, Vezzani A. Inflammation and reactive oxygen species as disease

modifiers in epilepsy. Neuropharmacology. 2020;167:107742.

43. Lugrin J, Rosenblatt-Velin N, Parapanov R, Liaudet L. The role of oxidative stress during inflammatory processes. Biol Chem. 2014;395(2):203-230.

44. Bozzi Y, Borrelli E. The role of dopamine signaling in epileptogenesis. Front Cell Neurosci. 2013;7. doi:10.3389/fncel.2013.00157/abstract

45. Poirier J, Baccichet A, Dea D, Gauthier S. Cholesterol synthesis and lipoprotein reuptake during synaptic remodelling in hippocampus in adult rats. Neuroscience. 1993;55(1):81-90.

46. de Freitas RM, do Nascimento KG, PMP F, Jordán J. Neurochemical changes on oxidative stress in rat hippocampus during acute phase of pilocarpine-induced seizures. Pharmacol Biochem Behav. 2010;94(3):341-345.

47. Scorza FA, Arida RM, Naffah-Mazzacoratti MG, Scerni DA, Calderazzo L, Cavalheiro EA. The pilocarpine model of epilepsy: what have we learned? An Acad Bras Cienc. 2009;81(3):345-365. doi:10.1590/s0001-37652009000300003

48. Rusina E, Bernard C, Williamson A. The kainic acid models of temporal lobe epilepsy. eNeuro. 2021;8(2): ENEURO.0337–20.2021. doi:10.1523/ENEURO.0337-20.2021

Supporting Information

Additional supporting information may be found online in the Supporting Information section at the end of the article.

Table S1. Enrichment analysis report. Enrichment by GO Processes. List of biological processes altered in the three animal models of mesial temporal lobe epilepsy.
Table S2. Enrichment analysis report. Enrichment by Pathway Maps. List of enriched pathways in three animal models of mesial temporal lobe epilepsy.
Table S3. Enrichment analysis report. Enrichment by GO Processes. List of biological processes altered in tissue from patients with mesial temporal lobe epilepsy.